

Induced NB-3 Limits Regenerative Potential of Serotonergic Axons after Complete Spinal Transection

Zhenhui Huang¹, Gao Yarong¹, Yasushi Shimoda², Kazutada Watanabe³, Yaobo Liu^{1, *}

¹Jiangsu Key Laboratory of Neuropsychiatric Diseases and Institute of Neuroscience,
Soochow University, Suzhou, Jiangsu, China.

²Department of Bioengineering, Nagaoka University of Technology, Niigata, Japan

³Nagaoka National College of Technology, Niigata, Japan

Zhenhui Huang, Ph.D.

Tel : 86-13205170421

Email : adam58433@163.com

Gao Yarong,

Tel : 86-18896508365

Email : 775459577@qq.com

Yasushi Shimoda, Ph.D.

Tel: 81-258-47-9423

Fax: 81-258-47-9400

Email : shimo@vos.nagaokaut.ac.jp

Kazutada Watanabe, Ph.D.

Tel : 81-258-47-9422 or 9013

Email : kazutada@vos.nagaokaut.ac.jp

This paper has been peer-reviewed and accepted for publication, but has yet to undergo copyediting and proof correction. The final published version may differ from this proof.

* Address correspondence to:

Yaobo Liu, Ph.D. M.D.

Tel: 86-512-65882526

Email: liuyaobo@suda.edu.cn

Abstract

NB-3 (contactin-6) is a member of the contactin family and has a wide range of roles during central nervous system development and disease. Here we found that NB-3 was simultaneously induced in the serotonergic raphespinal tract (sRST) axons and in the scar-forming cells after spinal cord injury (SCI). The regrowth of the sRST axons was promoted *in vivo* by blocking NB-3 expression in either sRST axons or scar-forming cells when post-traumatic axons of the sRST tried to penetrate the glial scar. NB-3 deficiency promoted synapse reformation between sRST regenerative axons and motor neurons and enhanced the potential for electrical activity of muscle contraction and motor coordination. *In vivo* evidence also suggested that NB-3 induction in both sRST axons and scar-forming cells was required to mediate NB-3 signaling inhibition of sRST axon regeneration after SCI. Our findings suggest that NB-3 protein is a potential molecular target for future SCI treatments.

Keywords: serotonergic raphespinal tract; NB-3; axonal regeneration; synapse reformation; motor coordination

Introduction

SPINAL CORD INJURIES (SCIs) are mainly caused by vehicle crashes, acts of violence, and sports activities and occur especially in the young adult population. Obviously, it is of high priority to regain motor function for those patients. Although attempts at complete restoration of voluntary motor functions after SCI have routinely failed, there are a great deal of promising intervention methods that target the repair of or improvement in the plasticity of motor circuits involved in motor function, such as enhancing the intrinsic abilities of neurons (Liu et al., 2010), stem cell grafting (Lu et al., 2012), reducing non-permissive environments for axonal regrowth (Oles et al., 2011), and implanting neural interfaces for functional restoration of spinal cord (Capogrosso et al., 2016). All of these have resulted in improvements in our understanding of the underlying molecular and cellular processes, which may lead to the development of novel therapeutic strategies for reconstruction of motor circuits involved in motor function.

The serotonergic raphespinal tract (sRST) has very important roles in modulating locomotion (Cabaj et al., 2016). The B1–B3 cell groups (*raphe magnus*, *raphe obscurus*, and *raphe pallidus*, respectively) of the caudal *raphe nucleus* (CRN) along the midline of the caudal medulla send descending axonal projections of the sRST to motor and some autonomic neurons in the spinal cord (Skagerberg et al., 1985). These axonal terminations are widely branched in the dorsal horn and among different motoneuronal cell groups at all spinal levels, especially at the thoracolumbar and upper sacral spinal levels. Axonal terminals of the sRST are found in lamina 1, lamina 2, and lamina 8–10 (Anderson et al., 1989). The main effects of the sRST are on spinal reflexes, and result from level-setting of motoneuronal membrane excitability (Heckman et al., 1999; Ghosh et al., 2015). After SCI, activation of 5-HT₂ receptors and 5-HT_{1A/7} receptors in the interneurons of central pattern generators (CPGs) or motor neurons (MNs) partially restores hindlimb movements during locomotion (Urszula et al., 2014). Both CPGs and MNs are essential elements of neuronal circuits that produce rhythmic motor patterns and direct left–right coordination, flexor–extensor antagonism, and stance–swing phase transitions (Kiehn et al., 2016). However, as few studies of the mechanisms regulating axonal regeneration of the post-traumatic sRST in rodents are commonly accepted in the field (Nikulina et al., 2004; Coles et al., 2011), and

additional efforts are needed to elucidate those molecules involved in axonal regrowth of the sRST and restoration of locomotor neural circuitry after spinal cord injury (SCI).

NB-3 (contactin-6) is a member of the contactin family and is expressed exclusively in the nervous system. NB-3 has a wide range of roles in neural development (Takeda et al, 2003; Sakurai et al, 2009, 2010; Huang et al, 2012). For instance, NB-3 interacts with close homolog of L1 (CHL1) and protein tyrosine phosphatase α (PTP α) to regulate the development of dendritic projections in the visual cortex (Ye et al, 2008). Additionally, NB-3 is involved in brain damage after cerebral ischemia (Huang et al, 2011) and is responsible for the regulation of axonal regeneration of corticospinal tracts after SCI (Huang et al., 2016).

Here we found that NB-3 signaling inhibited sRST regeneration after SCI. Knocked down NB-3 expression in either sRST axons or scar-forming cells enhanced the axonal regrowth of the sRST. NB-3 deficiency promoted the reconstruction of motor neural circuitry and partially restored locomotor movements.

Methods

Animals and surgeries

All the procedures were in accordance with the Institute of Neuroscience (Soochow University) guidelines for the use of experimental animals and were approved by the Institutional Animal Care and Use Committee at Soochow University. All mice were on a C57BL/6J background and were kept in the specific pathogen-free animal facility at Soochow University. NB-3-deficient mice were described previously (Takeda et al., 2003). Mice were used for surgery at the age of 10 weeks (22–24 g). Pentobarbital (40 mg/kg, i.p.) was injected to anesthetize the mice. Spinal T10 complete transections were carried out by modifying previously described methods (Liu et al., 2008; Huang et al, 2016). The spinal cord was transected bilaterally across its entire width and depth in the vertebral cavity with iridectomy microscissors. Then, a microknife was used to pass through the lesion site twice and press against the lateral and ventral sides of the vertebral cavity to ensure the completeness of the lesion. Sham operations were performed as follows: the dorsal vertebral lamina at spinal T10 segment was cut off, but the spinal cord itself was left intact. After these operations, the muscle layers, fascia, and the skin were

sequentially sutured. Urine was expressed by manual abdominal pressure twice per day until mice regained reflex bladder function.

Plasmid construction and cell lines

The cDNA template for an shRNA specific for the NB-3 coding sequence was 5'–CCGGGCTGCAAAGGATTCATCTATACTCGAGTATAGATGAATCCTTTGCAGCTTTTTTG–3', and the negative control (nc) was 5'–CCGGGCTTCTCCGAACGTGTCACGTTTTTTTG–3'. Both templates were subcloned into the vector pLKD-CMV-GFP-U6-shRNA (OBiO Inc.). The full-length NB-3 sequence (1–1028 aa) and the NB-3- Δ ECD sequence (997–1028 aa; ECD, extracellular domain) were subcloned into the vector pLenti-CMV-EGFP-P2A (OBiO Inc.).

Anterograde labeling

To examine NB-3 knockdown and overexpression in the sRST after SCI, 2–3 μ l of LV-NB-3 shRNA-GFP (OBiO Inc.) was injected into the CRN in wild-type mice, and an equal amount of LV-NB-3-EGFP (OBiO Inc.) was injected into the CRN in NB-3-deficient mice after drilling the skull above. The Hamilton syringe was left in place for 10 min after the injection in each trial. Mice were kept for 1 month before being sacrificed to examine the anterogradely labeled sRST.

Fluorogold (FG) retrograde labeling

To examine NB-3 induction in the sRST somas after SCI, 1 μ l of FG (2 mg/ml; Biotium) was injected into the sRST axonal termination areas (0.5, 2.5, 4.5, and 6.5 mm caudal to the T10 spinal segment; 0.8 and –0.8 mm lateral to the midline; and 0.8 mm below the dorsal surface of the spinal cord) of the raphespinal tract at the T10 segment of the spinal cord after transection or sham surgery. Mice were kept for another week before being sacrificed to examine retrogradely labeled sRST somas.

To examine the connections between regenerative serotonergic axons and MNs after SCI, 1 μ l of FG (Biotium) was injected into multiple sites of the gastrocnemius (GS) and tibialis anterior (TA) around the sural nerves, tibial nerves, and peroneal nerves in the hindlimbs to label MNs in L3–L4 spinal cord. Mice were kept for another week before being sacrificed to examine retrogradely labeled MNs.

Immunohistochemistry

Pentobarbital (40 mg/kg, i.p.) was injected to anesthetize the mice before sacrificing them. Mice were perfused with 4% paraformaldehyde (PFA; Sigma) in phosphate-buffered saline (PBS; pH 7.4; Sinoreagent). Brainstems and spinal cords were dissected out and washed with PBS. Then these tissues were soaked in 30% sucrose (Sinoreagent) overnight to replace PFA with sucrose. After that, tissues were embedded with Tissue-Tek O.C.T. Compound (Sakura Finetek) for cryosectioning. After cryosectioning, coronal sections (30 μm thick) of the brainstem were used for immunostaining. Sagittal sections (1.0 cm long) of lesioned and intact spinal cords were also obtained. Primary antibodies were used as follows: 5-HT (Sigma, S5545, 1:500), GFAP (DAKO, Z0334, 1:500; Chemicon, MAB360, 1:500), NB-3 (R&D, AF5890, 1:500), GFP (Invitrogen, A11120, 1:200), and Syn (Chemicon, AB9272, 1:500). Subsequently, the sections were incubated with secondary antibodies conjugated with Alexa 488, 555, or 647 (Invitrogen) overnight at 4°C. Images were acquired with a Zeiss 700 confocal microscope (Carl Zeiss Company) and processed and exported with the Zen software (Carl Zeiss Company).

Western blotting

To validate the overexpression efficiency of LV-NB-3-EGFP construct and knockdown efficiency of LV-NB-3 shRNA-GFP construct in injured spinal cords, a 2-mm-long region of the spinal tissue that contained the injection site was dissected from each spinal cord. Samples were lysed and then supersonically prepared for SDS-PAGE. After the electrophoresed proteins were transferred to PVDF membrane, blots were incubated with primary antibodies (NB-3, R&D, AF5890, 1:1000; GAPDH, Sigma, G9545, 1:1000; GFP, Invitrogen, A11120, 1:1000) and then with horseradish peroxidase-conjugated secondary antibodies (GE Healthcare) for visualization with Image Lab (Bio-Rad). Three mice were used in each group.

Rehabilitation device

A portable rehabilitation device built in-house was used for the SCI mice as they had difficulties in executing locomotive movements without upper body support (van den Brand et al., 2012). The upper body of the mouse was fastened to and lifted by the device

to enable the movement of its hindlimbs on the treadmill surface. The device also enabled the mice to carry out continuous locomotion on an automated moving treadmill.

Electromyography (EMG) recording

Three months after complete spinal transection, EMG recording electrodes were implanted in both the left and right soleus muscles of the hindlimbs. The disposable subdermal needle electrodes were made of Teflon-coated stainless-steel wire (Carefusion GmbH, Germany). The tips of the electrodes were poked through a cutaneous incision and were inserted into the appropriate muscle, with a distance of 1–2 mm maintained between the separated tips of the bipolar electrodes, which were secured by a suture (Urszula Sławinska et al., 2013). The ground electrode was placed under the skin on the back of the mouse. A wire loop, which was covered with dental cement and silicone, was left to prevent the electrodes from being pulled out from under the skin on the backs of the mice. Under the condition of complete spinal transection, stimulation of the afferents was used for inducing locomotion (Lev-Tov et al., 2010). To block muscle contraction and left–right coordination with a 5-HT receptor antagonist, intrathecal application of SB269970 (Selleck, S2849; 0.1–10 mg/kg in phosphate buffer saline) (Cabaj et al., 2016) or cyproheptadine (Selleck, S4635; 1–10 mg/kg in phosphate buffer saline) (Koschnitzky et al., 2014) was carried out. EMG recording (see below) was carried out immediately after intrathecal application of SB269970 or cyproheptadine. After the mice were sacrificed, electrode positions were visually verified in the muscles.

EMG analysis

During the locomotor-like movement test of the hindlimbs of the mice, the EMG activity of the hindlimb extensors (soleus) was recorded by Biopac MP150 (band pass, 0.01–1 kHz) and evaluated after digitization on the computer (sampling frequency, 2 kHz). At least 50 consecutive step cycles for the soleus muscles were measured, before the mean EMG activity onset from 50 consecutive step cycles was compared between the left and right hindlimb groups under different conditions. EMG activity was analyzed and quantified, and the phasing of EMG firing during locomotion was determined by circular statistics and represented as circular polar plots (Zar, 2000). To measure whether the

rhythm was lost in one hindlimb in one test, Rayleigh's circular test was used to determine whether the r values were clustered. The P -value in Rayleigh's test was calculated as follows: $p = \exp\{\sqrt{1 + 4N + 4(N^2 - R_n^2)} - (1 + 2N)\}$; where $R = \|\bar{r}\|$, $R_n = R \cdot N$. Dots outside the inner circle indicate the $p < 0.05$ significance level (Berens et al., 2009). The mean onset phases of the left and right EMG bursts in all tests were calculated and are presented as the red and green arrows, respectively. The formulas for the arrow phase calculation were as follows: $\alpha_i \text{ (radians)} = 2\pi \cdot \alpha_i \text{ (angle)}/360$; $a_i = (\cos \alpha_i; \sin \alpha_i)$; \bar{a} (arrow phase) = $1/N \cdot \sum a_i$. Motor coordination requires rhythmic movements in each soleus muscle and left-right alternation between the two hindlimbs during locomotion.

Quantification of axon intensity index

The projection length of sRST axons in the spinal cord was measured using Image J (NIH). In each sagittal section of injured spinal cord, dorso-ventral lines were drawn at -3.0 to 0 mm relative to the rostral lesion border (0 mm) and at 0 to 1 mm relative to the caudal lesion border (0 mm). SRST axons that intersected each line were counted. The axon intensity index at a specific position is a ratio of the intensity of sRST axons relative to the density of axons 3 mm rostral to the lesion border. Three sections that included the sRST axons were quantified for each mouse.

Analysis of synapse re-formation

Sections were collected from 0.5 mm rostral or 0.5 mm caudal to the spinal lesion site. Immunostaining with 5-HT and synaptophysin (syn) antibodies in those sections collected from FG retrograde labeled mice was carried out to detect synapses between 5-HT-positive raphespinal axons and FG-labeled MNs. In each coronal section, synapse numbers per neuron were determined by quantifying 5-HT-positive and syn-positive puncta on FG-positive neurons in randomly selected $70 \times 70 \mu\text{m}$ frames. Five representative sections were quantified for each mouse.

Statistical analysis

A two-tailed one-sample t-test was used for the single comparison between two groups. Rayleigh's circular test was used to determine whether the r values were clustered. Others were analyzed using a one- or two-way analysis of variance (ANOVA) followed by Fisher's least significant difference (LSD) post-test. Among all the experiments, no randomization was used. All analyses were carried out with Origin 8 (Originlab Software), GraphPad 6 Prism (GraphPad Software), and Matlab (Mathworks). All data are presented as the mean \pm SEM.

Results

Induction of NB-3 protein in the axons of the post-traumatic raphespinal tract and scar-forming cells

Complete spinal transection was performed at the T10 segment in NB-3^{+/+} mice to examine the pattern of induced expression of NB-3 protein in the somas and axons of the post-traumatic sRST after SCI. FG was injected into the lesion area of sham-injured and injured spinal cords to retrogradely label the somas of the sRST in the caudal raphe nuclei, where these axons originate (Fig. 1A). The mice were sacrificed 14 days post-injury (14 dpi) and examined by immunohistochemistry. NB-3 expression was induced in FG-labeled sRST somas of SCI mice (Fig. 1B, C, C1–C3) but was absent in sham-injured mice (Fig. 1D, E, E1–E3). At 14 dpi, NB-3 induction was detected at the distal portions of post-traumatic sRST axons and in the GFAP-positive glial scar (Fig. 1F–H, G1–G3, H1–H3). In contrast, sagittal sections of sham-operated spinal cord showed that NB-3 was undetectable in intact sRST axons (Fig. 1I–K, J1–J3, K1–K3). In addition, NB-3 was also undetectable in brainstems of sham-operated or injured NB-3^{-/-} mice (Supplementary Fig. 1A and B, A1–A4 and B1–B4; see online supplementary material at www.liebertpub.com) or in spinal cords of sham-operated or injured NB-3^{-/-} mice (Supplementary Fig. 1C and D, C1–C3 and D1–D3; see online supplementary material at www.liebertpub.com). Thus, NB-3 was induced in the somas and injured axons of the sRST and was simultaneously observed in the GFAP-positive glial scar after SCI. NB-3-positive cells in the glial scar were previously identified as being scar-forming cells and included astrocytes, fibroblasts, and pericytes (Huang et al., 2016).

Axonal regrowth of sRST axons in NB-3-deficient mice after SCI

To investigate whether NB-3 deficiency affects the regrowth of severed sRST axons, complete spinal transection was performed at the T10 segment in both NB-3^{+/+} and NB-3^{-/-} mice (Fig. 2A). In NB-3^{+/+} mice, post-traumatic sRST axons remained at the rostral lesion border, even 84 dpi (Fig. 2B–E). In contrast, the completely transected sRST axons in NB-3^{-/-} mice displayed obvious regrowth (Fig. 2F–I). Many 5-HT-positive sRST axons in NB-3^{-/-} mice spread out toward the lesion epicenter, and some even traversed the lesion epicenter and extended ~1 mm beyond the caudal lesion border (Fig. 2F, dashed line). Quantification of the axon intensity index at various distances from the lesion borders revealed significantly enhanced numbers of sRST axons in the injured spinal cords of NB-3^{-/-} mice from –0.2 to 0 mm to the rostral lesion border, and from 0 to 1.0 mm to the caudal lesion border as compared with NB-3^{+/+} mice (Fig. 2J; $p < 0.01$ for NB-3^{+/+} vs. NB-3^{-/-}; $n = 13$ mice). Thus NB-3 deficiency results in enhanced regrowth of post-traumatic sRST axons after SCI.

To determine whether the regrowth of sRST axons was due to axonal regeneration or axonal preservation, the time course of axonal extension was also analyzed in NB-3^{+/+} and NB-3^{-/-} mice (Supplementary Fig. 2; see online supplementary material at www.liebertpub.com). In NB-3^{+/+} mice at 28, 42, and 56 dpi, all the post-traumatic sRST axons remained at the rostral lesion border and did not penetrate into the lesion area (Supplementary Fig. 2A, C, and E; see online supplementary material at www.liebertpub.com). In contrast, post-traumatic sRST axons regrew as far as several millimeters toward the caudal lesion site in caudal spinal cord in NB-3^{-/-} mice. Moreover, the regrowing sRST axons appeared to be more robust in NB-3^{-/-} mice at 42 and 56 dpi compared with those in NB-3^{-/-} mice at 28 dpi (Supplementary Fig. 2B, D, and F; see online supplementary material at www.liebertpub.com). Quantification of the axon intensity index at various distances from the lesion borders revealed significantly enhanced numbers of sRST axons in NB-3^{-/-} mice as compared with NB-3^{+/+} mice at 28, 42, and 56 dpi (Supplementary Fig. 2G; $p < 0.01$ for NB-3^{+/+} 28 dpi vs. NB-3^{-/-} 28 dpi; $p < 0.01$ for NB-3^{+/+} 42 dpi vs. NB-3^{-/-} 42 dpi; $p < 0.01$ for NB-3^{+/+} 56 dpi vs. NB-3^{-/-} 56 dpi; $n = 10$ mice; see online supplementary material at www.liebertpub.com). Thus NB-3 deficiency-related

This paper has been peer-reviewed and accepted for publication, but has yet to undergo copyediting and proof correction. The final published version may differ from this proof.

Journal of Neurotrauma

Induced NB-3 Limits Regenerative Potential of Serotonergic Axons after Complete Spinal Transection (DOI: 10.1089/neu.2018.5652)

Downloaded by Univ Of Western Ontario from www.liebertpub.com at 09/09/18. For personal use only.

enhanced regrowth of post-traumatic sRST axons after SCI was not due to simple preservation of spared sRST axons but was instead due to axonal regeneration.

Blocking NB-3 expression in the sRST or scar-forming cells enhances regrowth of post-traumatic sRST axons

To further test our hypothesis, we injected LV-NB-3 shRNA-GFP into the spinal lesion site to knock down NB-3 expression in scar-forming cells. We observed a difference in sRST axons between LV-NB-3 shRNA-GFP and LV-NC-GFP (NC, negative control) infection in the completely transected spinal cord 84 dpi (Fig. 3A). In addition, LV-NC-EGFP and LV-NB-3 shRNA-EGFP constructs were validated *in vivo* from spinal cord lysates by western blotting (Fig. 3B; $p < 0.0001$ for NB-3^{-/-} vs. NB-3^{+/+} + NC in lesion site, $p = 0.001$ for NB-3^{-/-} vs. NB-3^{+/+} + NB-3 shRNA in lesion site, $p < 0.0001$ for NB-3^{+/+} + NC in lesion site vs. NB-3^{+/+} + NB-3 shRNA in lesion site; $n = 12$ mice). The 5-HT-positive post-traumatic axons that were in contact with LV-NC shRNA-GFP-infected scar-forming cells remained at the rostral lesion border, even 84 dpi (Fig. 3C–F). In contrast, substantial numbers of 5-HT-positive axons that contacted the LV-NB-3 shRNA-GFP-infected scar-forming cells extended toward the rostral lesion border and some even emerged from the caudal lesion border 84 dpi (Fig. 3G–J). Quantification of the axon intensity index confirmed that injecting LV-NB-3 shRNA-GFP into the spinal lesion site showed significantly increased numbers of sRST axons in the injured spinal cords from –0.2 to 0 mm to the rostral lesion border and from 0 to 1.0 mm to the caudal lesion border as compared with lesion injection of LV-NC-GFP (Fig. 3K; $p < 0.01$ for NB-3^{+/+} + NC in lesion site vs. NB-3^{+/+} + NB-3 shRNA in lesion site; $n = 12$ mice). Additionally, regeneration of sRST axons was observed following NB-3 knockdown in the CRN of NB-3^{+/+} mice (Supplementary Fig. 3A–D; see online supplementary material at www.liebertpub.com) or following NB-3 knockdown in both the CRN and spinal lesion site of NB-3^{+/+} mice (Supplementary Fig. 3E–H; see online supplementary material at www.liebertpub.com). Quantification of the intensity index of sRST axons also confirmed our observation (Supplementary Fig. 3Q; *n.s.* for NB-3^{+/+} + NB-3 shRNA in CRN vs. NB-3^{+/+} + NB-3 shRNA in CRN and lesion site; $n = 10$ mice; see online supplementary material at www.liebertpub.com). Thus knockdown of NB-3 induction in sRST axons or scar-forming

This paper has been peer-reviewed and accepted for publication, but has yet to undergo copyediting and proof correction. The final published version may differ from this proof.

cells efficiently interrupted the inhibitory signal transduction and led to the regrowth of 5-HT-positive post-traumatic axons.

To further verify the effect of interrupting NB-3 induction in scar-forming cells on the regrowth of 5-HT-positive post-traumatic axons, we tried to restore NB-3 expression in the spinal lesions of NB-3^{-/-} mice (Fig. 4A). The constructs LV-NC-EGFP and LV-NB-3ΔECD-EGFP, the latter of which encodes NB-3 without the extracellular domain, were validated *in vivo* using spinal cord lysates and western blotting (Fig. 4B; $p = 0.729$ for NB-3^{+/+} vs. NB-3^{-/-} + NB-3 in lesion site, $p < 0.0001$ for NB-3^{-/-} + NB-3 in lesion site vs. NB-3^{-/-} + NB-3ΔECD in lesion site, $p < 0.0001$ for NB-3^{-/-} + NB-3 in lesion site vs. NB-3^{-/-} + NC in lesion site; $n = 12$ mice). We injected the lentivirus overexpressing full-length NB-3 (LV-NB-3-EGFP) into spinal lesion sites of NB-3^{-/-} mice (Fig. 4C–F). We injected LV-NB-3ΔECD-EGFP into spinal lesion sites of NB-3^{-/-} mice (Fig. 4G–J). Spinal injection of LV-NC-EGFP was used as a control (Fig. 4K–N). Under all of these conditions, no interruption in sRST axon regeneration was observed, which was confirmed by quantification of the axon intensity index (Fig. 4O; *n.s.* for NB-3^{-/-} + NB-3 in lesion site vs. NB-3^{-/-} + NB-3ΔECD in lesion site; *n.s.* for NB-3^{-/-} + NB-3 in lesion site vs. NB-3^{-/-} + NC in lesion site; *n.s.* for NB-3^{-/-} + NB-3ΔECD in lesion site vs. NB-3^{-/-} + NC in lesion site; $n = 13$ mice). Additionally, interruption of sRST regeneration was not observed following NB-3 overexpression in the CRN of NB-3^{-/-} mice (Supplementary Fig. 3I–L; see online supplementary material at www.liebertpub.com). However, the inhibitory effect of NB-3 on axonal regeneration was restored following NB-3 overexpression in both the CRN and spinal lesion site of NB-3^{-/-} mice (Supplementary Fig. 3I–P; see online supplementary material at www.liebertpub.com). Quantification of the intensity index of sRST axons at various distances from the lesion borders also confirmed our observation (Supplementary Fig. 3Q; $p < 0.01$ for NB-3^{-/-} + NB-3 in CRN vs. NB-3^{-/-} + NB-3 in CRN and lesion site; $n = 10$ mice; see online supplementary material at www.liebertpub.com). Therefore, NB-3 induction in both sRST axons and scar-forming cells was necessary for mediating the transduction of this inhibitory signal.

This paper has been peer-reviewed and accepted for publication, but has yet to undergo copyediting and proof correction. The final published version may differ from this proof.

NB-3-deficient mice exhibit synapse reformation after SCI

Immunohistochemistry was performed to detect synapse reformation in the spinal cords 84 dpi (Fig. 5A). In NB-3^{+/+} and NB-3^{-/-} mice, normal numbers of synaptophysin (syn)-positive synapses were detected between sRST axons and MNs in the spinal cord 0.5 mm rostral to the lesion sites (Fig. 5B, C). In NB-3^{+/+} mice, T10 complete spinal transection substantially reduced the number of syn-positive synapses in the caudal spinal cord as compared with the number of syn-positive synapses in the rostral spinal cord (Fig. 5D). In contrast, syn-positive synapses were reformed between regenerative sRST axons and MNs in the distal spinal cord of NB-3^{-/-} mice 84 dpi (Fig. 5E). Quantification of the number of syn-positive synapses per neuron confirmed the reformation of syn-positive synapses between regenerative sRST axons and MNs in the distal spinal cord of the NB-3^{-/-} mice (Fig. 5F; $p = 0.196$ for rostral NB-3^{+/+} vs. rostral NB-3^{-/-}, $p < 0.0001$ for rostral NB-3^{+/+} vs. caudal NB-3^{+/+}, $p < 0.0001$ for rostral NB-3^{-/-} vs. caudal NB-3^{-/-}, $p < 0.0001$ for caudal NB-3^{+/+} vs. caudal NB-3^{-/-}; $n = 10$ mice).

NB-3-deficient mice show improved EMG activity and coordination after SCI

EMG was used to examine the locomotion improvement brought about by axonal regeneration of sRST axons. Recording electrodes were implanted in both soleus muscles of the hindlimbs, and locomotion was induced by a rehabilitation facility (Fig. 6A) (Van et al., 2012). In NB-3^{-/-} mice, T10 complete spinal transection totally abolished muscle contraction and motor coordination immediately after injury, but these were partially restored 84 dpi, in comparison with the total abolishment of muscle contraction and motor coordination in NB-3^{+/+} mice 84 dpi (Fig. 6B, C). In contrast, the restored muscle contraction and left-right coordination in NB-3^{-/-} mice was partially abolished by the 5-HT₇ receptor antagonist SB269970 (Cabaj et al., 2016), which inhibits synaptic transmission between the serotonergic axons and CPGs (Fig. 6D). In addition, the 5-HT₂ receptor antagonist cyproheptadine abolished almost all the restored contractions and left-right coordination in NB-3^{-/-} mice (Fig. 6E), presumably by inhibiting synaptic transmission between serotonergic axons and MNs or CPGs. Quantification of EMG activity confirmed the restored contractions and left-right coordination in NB-3^{-/-} mice, which was inhibited by 5-HT receptor antagonists (Fig. 6F;

$n = 10$ mice). These results demonstrated that the NB-3 deficiency led to the improvement in EMG activity and left–right coordination. The increase in EMG activation and left–right coordination supported the morphological evidence of sRST regrowth and synapse reformation in the injured spinal cords of NB-3^{-/-} mice.

Discussion

The molecular signaling pathways mediating axonal regeneration of the post-traumatic sRST in rodents have not been well elucidated. cAMP-related signaling molecules (Nikulina et al., 2004), Nogo (Kim et al., 2004), and chondroitin sulfate proteoglycans (CSPGs) (Coles et al., 2011) have all been reported to be involved in the axonal regeneration of the sRST. Our present work demonstrated that NB-3 induction is involved in inhibitory signal transduction to sRST axons after SCI. Additionally, our previous work demonstrated that PTEN/mTOR activity is downregulated in corticospinal neurons by NB-3 *trans*-homophilic interactions between post-traumatic corticospinal axons and scar-forming cells (Huang et al., 2016). However, there has as yet been no evidence that modulation of the PTEN/mTOR signaling pathway is relevant for sRST regeneration in rodents after SCI (Basso et al., 1995). This suggests that the molecules downstream of the NB-3 signaling pathway that regulate axonal regeneration of the sRST still needed to be explored.

To investigate whether this signaling inhibition during sRST regeneration requires NB-3 induction in both post-traumatic sRST axons and scar-forming cells, we tried to inject LV-NB-3 shRNA into either the CRN or the spinal lesion site in NB-3^{+/+} mice and to inject LV-NB-3 or LV-NB-3ΔECD into either the CRN or the spinal lesion site in NB-3^{-/-} mice. However, ~ 90% of the mice with CRN injections died before the planned time points. It is highly likely that brainstem manipulations typically trigger brainstem bleeding or epileptiform activity and lead to acute respiratory failure (Feldman et al., 2006; Liang et al., 2015), resulting in a high mortality rate after viral injection into the CRN. Albeit with a very low survival rate (10%) for CRN-injected mice, we thus verified the inhibitory role of NB-3 either with NB-3 shRNA expression in the CRN of NB-3^{+/+} mice or with NB-3 shRNA expression in both the CRN and spinal lesion site of NB-3^{+/+} mice. We also verified the inhibitory role of NB-3 either with NB-3 overexpression in the CRN of NB-3^{-/-} mice or with

This paper has been peer-reviewed and accepted for publication, but has yet to undergo copyediting and proof correction. The final published version may differ from this proof.

NB-3 overexpression in both the CRN and spinal lesion site of NB-3^{-/-} mice. Taken together, these findings demonstrated that NB-3 induction in both sRST axons and scar-forming cells was necessary for mediating the transduction of this inhibitory signal.

Contactin family member NB-3, which includes an extracellular domain consisting of six IgG-like domains and four FNIII-like domains, is anchored to the cell membrane by a glycosyl-phosphatidylinositol (GPI)-anchor (Shimoda et al., 2009). Contactin-4, -5, and -6, using a binding site that includes their second and third Ig repeats, interact with protein tyrosine phosphatase receptors; these binding sites may also be involved in NB-3 homophilic interactions (Bouyain et al., 2010). Based on our observation that the inhibition of NB-3 induction leads to axonal regeneration after SCI, this extracellular domain is a potential molecular target for interrupting the NB-3 signaling. Although the crystal structures of fibronectin-like domain 1–3 of human contactin-5 (<http://www.rcsb.org/pdb/explore/explore.do?structureId=5E52>), and the crystal structures of the complexes of the PTP receptor (Z/G) and distinct member of contactin family (Contactin-4, -5 or -6) (Bouyain et al., 2010)—have been reported, crystallographic identification is still required to locate the specific epitopes in the NB-3 protein. However, computational prediction and point-mutation analyses could provide insights into the extracellular epitopes of the NB-3 protein that would facilitate the design and testing of functional blocking antibodies or chemical antagonists. This potential molecular target may form the basis of future methods for treating SCI.

There have been increasing reports indicating the functionally supportive role of tissue grafts containing progenitor-derived astrocytes mediated extensive axon regrowth (Shih et al., 2014; Nguyen, et al., 2017), besides selective disruption of astrocyte during gliosis attenuates rather than promotes axon regrowth following SCI (Sofroniew, 2015; Anderson et al. 2016). In this study, we have also noticed the potential involvement of NB-3 deficiency in sparing astrocytes at the lesion site and/or promoting astrocyte migration to the lesion site, whereas some of regenerative 5-HT axons were associated with glial processes (Fig. 2 and Supplementary Fig. 2). It suggests the possibility that NB-3 deficiency provides an astrocyte-based permissive substrate, which partially contributing to 5-HT axon regeneration. Moreover, recent studies have revealed the molecular signals in

regulation of reactive astrocyte migration after injury. For instance, astrocyte-specific N-cadherin deficiency inevitably leads to the abnormal astrocyte migration (Kanemaru et al., 2013; Pégliion et al., 2012). Inhibition of integrin–N-cadherin signaling pathway interrupts the interaction between reactive astrocyte and type I collagen, and indeed results in axonal regrowth and functional recovery after SCI (Hara et al., 2017). Thus we speculate that the unidentified signaling pathway might be activated in regulation of the sparing astrocytes or promoting migration of astrocytes at the spinal lesion site of NB-3 deficient mouse. Nevertheless, further investigations remain necessary to elucidate the mechanism underlying NB-3 deficiency leading to regrowth of the 5-HT axons after SCI in the future.

Acknowledgements

Our study was financially supported by the National Natural Sciences Foundation of China (numbers 81330026, 81771330, 31271259), the National Key Basic Research Development Program of the Ministry of Science and Technology of China (973 Program, 2013CB945600), a project funded by the Priority Academic Program Development of Jiangsu Higher Education Institutions, and Key Research and Development Plan of Jiangsu Province (BE2018654).

Author Disclosure Statement

The authors declare no competing financial interests.

References

1. Anderson C.R., McLachlan E.M., and Srb-Christie O. (1989). Distribution of sympathetic preganglionic neurons and monoaminergic nerve terminals in the spinal cord of the rat. *J. Comp. Neurol.* **283**, 269–284.
2. Anderson, M.A., Burda, J.E., Ren, Y., Ao, Yan, O’Shea, T.M., Riki, K., Coppola, G., Khakh, B.S., Deming, T.J., and Sofroniew, M.V. (2016). Astrocyte scar formation aids central nervous system axon regeneration. *Nature* **532**, 195–200.
3. Basso, D.M., Beattie, M.S., and Bresnahan, J.C. (1995). A sensitive and reliable locomotor rating scale for open field testing in rats. *J. Neurotrauma* **12**, 1–21.
4. Berens, P. (2009). Circstat: a matlab toolbox for circular statistics. *J. Stat. Softw.* **31**, 1–21.
5. Blackmore, M.G., and Bixby, J.L. (2012). Krüppel-like Factor 7 engineered for transcriptional activation promotes axon regeneration in the adult corticospinal tract. *P. Natl. Acad. Sci. USA*, **109**, 7517–7522.
6. Bouyain S., Watkins, D.J. (2010). The protein tyrosine phosphatases ptpz and ptpg bind to distinct members of the contactin family of neural recognition molecules. *P. Natl. Acad. Sci. USA*, **107**, 2443-2448.
7. Cabaj, A.M., Majczyński, H., Couto, E., Gardiner, P.F., Stecina, K., Sławińska, U., and Jordan, L.M. (2016). Serotonin controls initiation of locomotion and afferent modulation of coordination via 5-HT₇ receptors in adult rats. *J. Physiol.* 10.1113/JP272271.
8. Capogrosso, M., Milekovic, T., Borton, D., Wagner, F., Moraud, E. M., and Mignardot, J. B., et al. (2016). A brain–spine interface alleviating gait deficits after spinal cord injury in primates. *Nature*, **539**, 284–288.
9. Dias D.O., Kim H., Holl D., et al. (2018) Reducing pericyte-derived scarring promotes recovery after spinal cord injury. *Cell*, **173**, 153-165.
10. Du, K., Zheng, S., Zhang, Q., Li, S., Gao, X., Wang, J., Jiang, L., and Liu, K. (2015). Pten deletion promotes regrowth of corticospinal tract axons 1 year after spinal cord injury. *J. Neurosci.* **35**, 9754-9763.
11. Faulkner, J.R., Herrmann, J.E., Woo, M.J., Tansey, K.E., Doan, N.B., and Sofroniew, M.V. (2004). Reactive Astrocytes Protect Tissue and Preserve Function after Spinal Cord Injury. *J. Neurosci.* **24**, 2143–2155.

This paper has been peer-reviewed and accepted for publication, but has yet to undergo copyediting and proof correction. The final published version may differ from this proof.

Journal of Neurotrauma

Induced NB-3 Limits Regenerative Potential of Serotonergic Axons after Complete Spinal Transection (DOI: 10.1089/neu.2018.5652)

Downloaded by Univ Of Western Ontario from www.liebertpub.com at 09/09/18. For personal use only.

12. Feldman, J.L., Del Negro, C.A. (2006). Looking for inspiration: new perspectives on respiratory rhythm. *Nat. Rev. Neurosci.* **7**(3), 232–241.
13. Fry, E.J., Chagnon, M.J., Lopez-Vales, R., Tremblay, M.L., and David, S. (2010). Corticospinal tract regeneration after spinal cord injury in receptor protein tyrosine phosphatase sigma deficient mice. *Glia* **58**, 423–433.
14. Ghosh, M., Pearse, D.D. (2015). The role of the serotonergic system in locomotor recovery after spinal cord injury. *Front. Neural Circuits* **8**, 1–14.
15. Göritz, C., Dias, D.O., Tomilin, N., Barbacid, M., Shupliakov, O., Frisé, J. (2011). A pericyte origin of spinal cord scar tissue. *Science* **333**, 238–242.
16. Hara M., Kobayakawa K., Ohkawa Y., Kumamaru H., Yokota K., Saito T., Kijima K., Yoshizaki S., Harimaya K., Nakashima Y., Okada S. (2017). Interaction of reactive astrocytes with type I collagen induces astrocytic scar formation through the integrin-N-cadherin pathway after spinal cord injury. *Nature Medicine*, **23**, 818–828.
17. Heckman, C.J., and Lee, R.H. (1999). Synaptic integration in bistable motoneurons. *Prog. Brain Res.* **123**, 49–56.
18. Herrmann, J.E., Imura, T., Song, B., Qi, J., Ao, Y., Nguyen, T.K., Korsak, R.A., Takeda, K., Akira, S., and Sofroniew, M. (2008). STAT3 is a critical regulator of astrogliosis and scar formation after spinal cord injury. *J. Neurosci.* **28**, 7231–7243.
19. Huang, Z.H., Yu, Y., Shimoda, Y., Watanabe, K., and Liu, Y.B. (2012). Loss of neural recognition molecule NB-3 delays the normal projection and terminal branching of developing corticospinal tract axons in the mouse. *J. Comp. Neurol.* **520**, 1227–1245.
20. Huang, Z., Gao, Y., Sun, Y., Zhang, C., Yin, Y., Shimoda, Y., Watanabe, K., and Liu, Y. (2016). NB-3 signaling mediates the cross-talk between post-traumatic spinal axons and scar-forming cells. *Embo J.* **35**, 1745–1765.
21. Jakovcevski, I., Wu, J., Karl, N., Leshchyns'ka, I., Sytnyk, V., Chen, J., Irintchev, A., and Schachner, M. (2007). Glial scar expression of CHL1, the close homolog of the adhesion molecule L1, limits recovery after spinal cord injury. *J. Neurosci.* **27**, 7222–7233.
22. Kanemaru, K., Jun K., Hiroshi S., Kenzo H., Yohei O., and Masamitsu I. (2013) Calcium-dependent N-cadherin up-regulation mediates reactive astrogliosis and neuroprotection after brain injury. *Proc. Natl. Acad. Sci. USA* **110**, 11612–11617.

23. Kiehn, O. (2016). Decoding the organization of spinal circuits that control locomotion. *Nat. Rev. Neurosci.* **17**, 224–238.
24. Kim, J.E., Liu, B.P., Park, J.H., and Strittmatter, S.M. (2004). Nogo-66 receptor prevents raphespinal and rubrospinal axon regeneration and limits functional recovery from spinal cord injury. *Neuron* **44**, 439–451.
25. Koschnitzky J.E., Quinlan K.A., Lukas T.J., et al. (2016). Effect of fluoxetine on disease progression in a mouse model of ALS. *Journal of Neurophysiology*, **111**, 2164-2176.
26. Lang, B.T., Cregg, J.M., DePaul, M.A., Tran, A.P., Xu, K., Dyck, S.M., Madalena, K.M., Brown, B.P., Weng, Y.L., Li, S., Karimi-Abdolrezaee, S., Busch, S.A., Shen, Y., and Silver, J. (2011). Modulation of the proteoglycan receptor PTP σ promotes recovery after spinal cord injury. *Nature* **518**, 404–408.
27. Lang, C., Bradley, P.M., Jacobi, A., Kerschensteiner, M., and Bareyre, F.M. (2013). STAT3 promotes corticospinal remodelling and functional recovery after spinal cord injury. *EMBO Rep.* **14**, 931–937.
28. Lee, J.K., Chow, R., Xie, F., Chow, S.Y., Tolentino, K.E., and Zheng, B. (2010). Combined genetic attenuation of myelin and semaphorin-mediated growth inhibition is insufficient to promote serotonergic axon regeneration. *J. Neurosci.* **30**, 10899-10904.
29. Lev-Tov, A., Etlin, A., Blivis, D. (2010). Sensory-induced activation of pattern generators in the absence of supraspinal control. *Ann. N.Y. Acad. Sci.* **1198**, 54–62.
30. Liang, H., Wang, S., Francis, R., Whan, R., Watson, and C., Paxinos, G. (2015). Distribution of raphespinal fibers in the mouse spinal cord. *Mol. Pain* **11**, 1–11.
31. Liu, K., Lu, Y., Lee, J.K., Samara, R., Willenberg, R., Sears-Kraxberger, I., Tedeschi, A., Park, K.K., Jin, D., Cai, B., Xu, B., Connolly, L., Steward, O., Zheng, B., and He, Z. (2010). PTEN deletion enhances the regenerative ability of adult corticospinal neurons. *Nat. Neurosci.* **13**, 1075–1081.
32. Lu, P., Wang, Y., Graham, L., McHale, K., Gao, M., Wu, D., Brock, J., Blesch, A., Rosenzweig, E.S., Havton, L.A., Zheng, B., Conner, J.M., Marsala, M., and Tuszynski, M.H. (2012). Long-distance growth and connectivity of neural stem cells after severe spinal cord injury: Cell-intrinsic mechanisms overcome spinal inhibition. *Cell.* **150**, 1264-1273.

33. Maier, I. C., Ichiyama, R. M., Courtine, G., Schnell, L., Lavrov, I., Edgerton, V. R., and Schwab, M.E. (2009). Differential effects of anti-nogo-a antibody treatment and treadmill training in rats with incomplete spinal cord injury. *Brain* **132**, 1426–1440.
34. McLean, J., Batt, J., Doering, L.C., Rotin, D., and Bain, J.R. (2002). Enhanced rate of nerve regeneration and directional errors after sciatic nerve injury in receptor protein tyrosine phosphatase sigma knock-out mice. *J. Neurosci.* **22**, 5481–5491.
35. Nguyen H.X., Hooshmand M.J., Saiwai H., Maddox J., Salehi A., Lakatos A., Nishi R.A., Salazar D., Uchida N., Anderson A.J. (2017) Systemic neutrophil depletion modulates the migration and fate of transplanted human neural stem cells to rescue functional repair. *J. Neurosci.* **37**, 9269–9287.
36. Nikulina, E., Tidwell, J.L., Dai, H.N., Bregman, B.S., and Filbin, M.T. (2004). The phosphodiesterase inhibitor rolipram delivered after a spinal cord lesion promotes axonal regeneration and functional recovery. *Proc. Natl. Acad. Sci. U. S. A.* **101**, 8786-8790
37. Okada, S., Nakamura, M., Katoh, H., Miyao, T., Shimazaki, T., Ishii, K., Yamane, J., Yoshimura, A., Iwamoto, Y., Toyama, Y., and Okano, H. (2006). Conditional ablation of Stat3 or Socs3 discloses a dual role for reactive astrocytes after spinal cord injury. *Nat. Med.* **12**, 829–834.
38. Oles, C.H., Shen, Y., Tenney, A.P., Siebold, C., Sutton, G.C., Lu, W., Gallagher, J.T., Jones, E.Y., Flanagan, J.G., and Aricescu, A.R. (2011). Proteoglycan-specific molecular switch for RPTPsigma clustering and neuronal extension. *Science*, **332**, 484–488.
39. Park, K.K., Liu, K., Hu, Y., Smith, P.D., Wang, C., Cai, B., Xu, B., Connolly, L., Kramvis, I., Sahin, M., and He, Z. (2008). Promoting axon regeneration in the adult CNS by modulation of the PTEN/mTOR pathway. *Science* **322**, 963–966.
40. Pégliion, F. & Etienne-Manneville, S. (2012). N-cadherin expression level as a critical indicator of invasion in non-epithelial tumors. *Cell Adh Migr.* **6**, 327–332.
41. Sakurai, K., Toyoshima, M., Ueda, H., Matsubara, K., Takeda, Y., Karagogeos, D., Shimoda, Y., and Watanabe, K. (2009). Contribution of the neural cell recognition molecule NB-3 to synapse formation between parallel fibers and Purkinje cells in mouse. *Dev. Neurobiol.* **69**, 811–824.

This paper has been peer-reviewed and accepted for publication, but has yet to undergo copyediting and proof correction. The final published version may differ from this proof.

42. Sakurai, K., Toyoshima, M., Takeda, Y., Shimoda, Y., and Watanabe, K. (2010). Synaptic formation in subsets of glutamatergic terminals in the mouse hippocampal formation is affected by a deficiency in the neural cell recognition molecule NB-3. *Neurosci. Lett.* **473**, 102–106.
43. Sapieha, P.S., Duplan, L., Uetani, N., Joly, S., Tremblay, M.L., Kennedy, T.E., and DiPolo, A., (2005). Receptor protein tyrosine phosphatase sigma inhibits axon regrowth in the adult injured CNS. *Mol. Cell. Neurosci.* **28**, 625–635.
44. Shen, Y., Tenney, A.P., Busch, S.A., Horn, K.P., Cuascut, F.X., Liu, K., He, Z., Silver, J., and Flanagan J.G. (2009). PTPsigma is a receptor for chondroitin sulfate proteoglycan, an inhibitor of neural regeneration. *Science* **326**, 592–596.
45. Shih C.H., Lacagnina M., Leuer-Bisciotti K., Pröschel C. (2014) Astroglial-derived periostin promotes axonal regeneration after spinal cord injury. *J. Neurosci.*, **34**, 2438–2443.
46. Shimoda, Y., Watanabe, K. (2009). Contactins: emerging key roles in the development and function of the nervous system. *Cell Adh. Migr.* **3**, 64-70.
47. Silver, J., Miller, J.H. (2004). Regeneration beyond the glial scar. *Nat., Rev. Neurosci.* **5**, 146–156.
48. Sofroniew, M.V. (2009). Molecular dissection of reactive astrogliosis and glial scar formation. *Trends. Neurosci.* **32**, 638–647.
49. Sofroniew, M.V. (2015) Astrocyte barriers to neurotoxic inflammation. *Nat. Rev. Neurosci.* **16**, 249–263.
50. Skagerberg, G., and Björklund, A. (1985). Topographic principles in the spinal projections of serotonergic and non-serotonergic brainstem neurons in the rat. *Neuroscience* **15**, 445–480.
51. Sun, F., Park, K.K., Belin, S., Wang, D., Lu, T., Chen, G., Zhang, K., Yeung, C., Feng, G., Yankner, B.A., and He, Z. (2011). Sustained axon regeneration induced by co-deletion of PTEN and SOCS3. *Nature* **480**, 372–375.
52. Takeda, Y., Akasaka, K., Lee, S., Kobayashi, S., Kawano, H., Murayama, S., Takahashi, N., Hashimoto, K., Kano, M., Asano, M., Sudo, K., Iwakura, Y., and Watanabe, K. (2003). Impaired motor coordination in mice lacking neural recognition molecule NB-3 of the contactin/F3 subgroup. *J. Neurobiol.* **56**, 252–265.

53. Thompson, K.M., Uetani, N., Manitt, C., Elchebly, M., Tremblay, M.L., and Kennedy, T.E. (2003). Receptor protein tyrosine phosphatase sigma inhibits axonal regeneration and the rate of axon extension. *Mol. Cell. Neurosci.* **23**, 681–692.
54. Wanner, I.B., Anderson, M.A., Song, B., Levine, J., Fernandez, A., Gray-Thompson, Z., Ao, Y., and Sofroniew, M.V. (2013). Glial Scar Borders Are Formed by Newly Proliferated, Elongated Astrocytes That Interact to Corral Inflammatory and Fibrotic Cells via STAT3-Dependent Mechanisms after Spinal Cord Injury. *J. Neurosci.* **33**, 12870–12886.
55. Urszula, S., Krzysztof, M., and Larry, M.J. (2014). 5-HT₂ and 5-HT₇ receptor agonists facilitate plantar stepping in chronic spinal rats through actions on different populations of spinal neurons. *Front. Neural Circuits.* **8**, 95.
56. van den Brand, R., Heutschi, J., Barraud, Q., DiGiovanna, J., Bartholdi, K., Huerlimann, M., Friedli, L., Vollenweider, I., Moraud, E.M., Duis, S., Dominici, N., Micera, S., Musienko, P., and Courtine, G. (2012). Restoring voluntary control of locomotion after paralyzing spinal cord injury. *Science* **336**, 1182–1185.
57. Wojtowicz, W.M., Flanagan, J.J., Millard, S.S., and Zipursky, S.L. (2004). Alternative splicing of *Drosophila* Dscam generates axon guidance receptors that exhibit isoform-specific homophilic binding. *Cell* **118**, 619–633.
58. Zar, J.H. (2000). *Biostatistical analysis*. Englewood Cliffs, NJ: Prentice-Hall.
59. Zukor, K., Belin, S., Wang, C., Keelan, N., Wang, X., and He, Z. (2013). Short Hairpin RNA against PTEN Enhances Regenerative Growth of Corticospinal Tract Axons after Spinal Cord Injury. *J. Neurosci.* **33**, 15350–15361.

This paper has been peer-reviewed and accepted for publication, but has yet to undergo copyediting and proof correction. The final published version may differ from this proof.

FIGURE LEGENDS

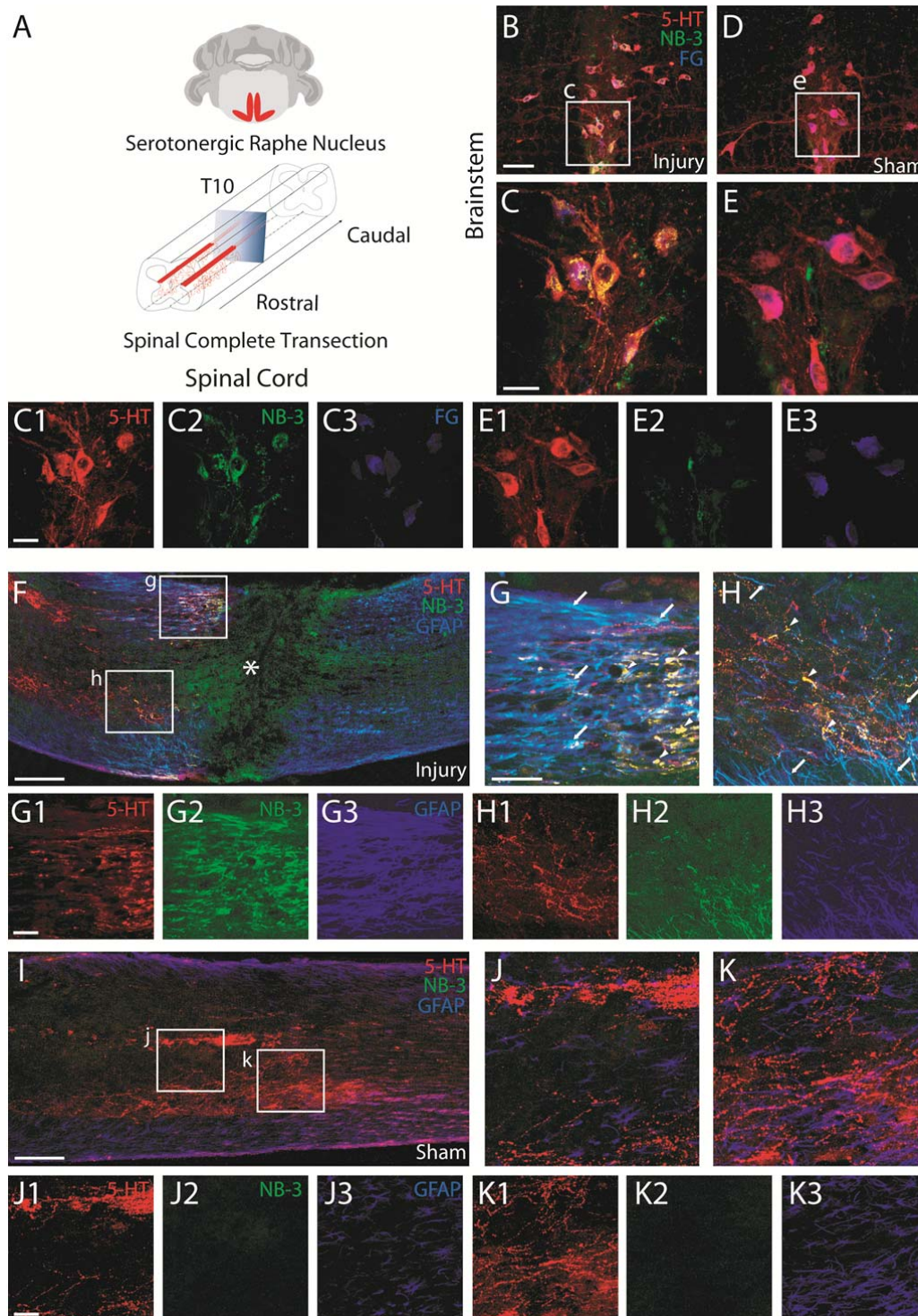


Fig. 1. Induced expression of NB-3 in somas and axons of serotonergic raphespinal tract and scar-forming cells after SCI. **(A)** Diagram of the serotonergic raphe nucleus at the level

of the brainstem and the sRST axons at the spinal lesion site of the injured spinal cord (in red). **(B–E)** FG (blue) was used to retrogradely label sRST somas. A 5-HT antibody (red) was used to label sRST somas and axons. NB-3 expression in sRST somas 14 dpi in injured **(B and C)** and sham-operated **(D and E)** NB-3^{+/+} mice. **C and E:** High-magnification images of boxed areas in **(B and D)**, respectively. **C1–C3 and E1–E3:** Splitting of the multichannel images from **(C and E)**. **(F–K)** Co-immunostaining of 5-HT (red), NB-3 (green), and GFAP (blue) in spinal cord from injured **(F–H)** and sham-operated **(I–K)** NB-3^{+/+} mice 14 dpi. **G–H and J–K:** High-magnification images of boxed areas in **(F and I)**, respectively. **G1–G3, H1–H3, J1–J3, and K1–K3:** Splitting of the multichannel images from **(G, H, J, and K)**, respectively. Arrows indicate NB-3 induction in the glial scar; arrowheads indicate NB-3 induction in sRST axons; the asterisk indicates the lesion epicenter. Scale bars, 50 μm **(B and D)**, 30 μm **(C, E, C1–C3, E1–E3)**, 250 μm **(F and I)**, 80 μm **(G–H, G1–G3, H1–H3, J–K, J1–J3, K1–K3)**.

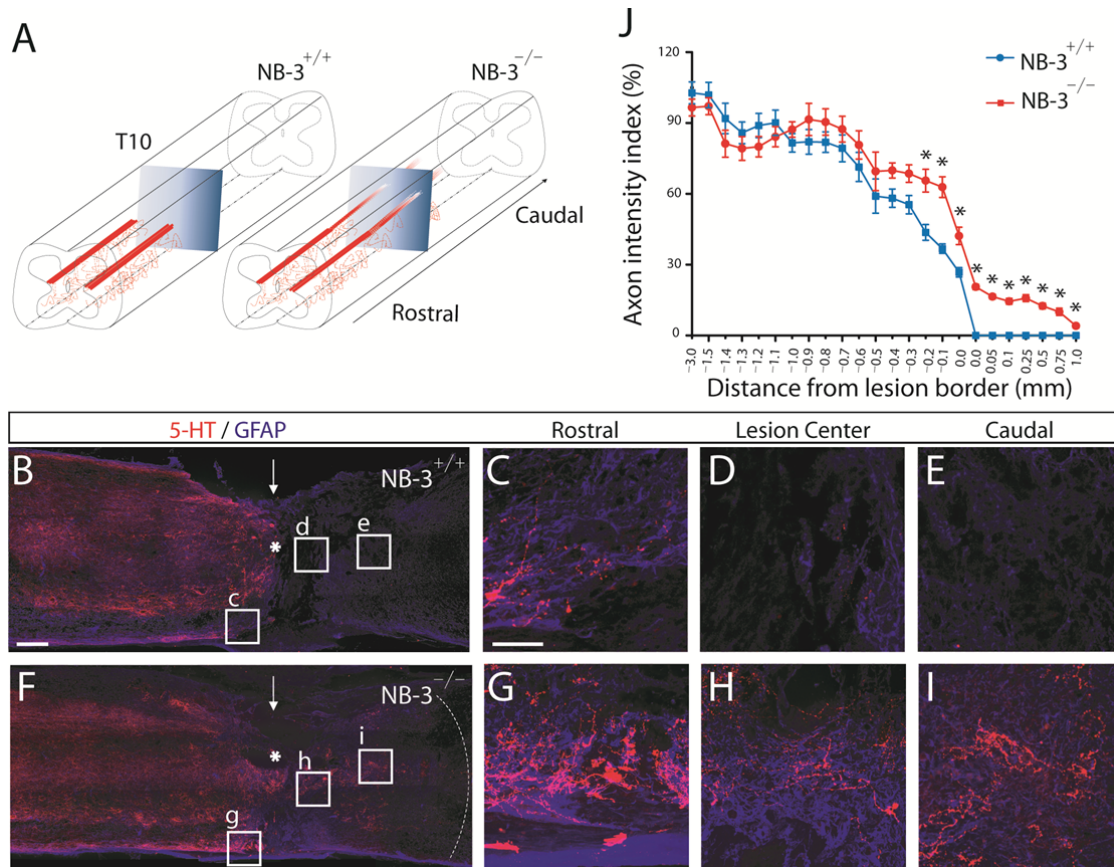


Fig. 2. NB-3 deficiency leads to enhanced regrowth of post-traumatic sRST axons. **(A)** Diagram of sRST axons at the spinal lesion sites of NB-3^{+/+} and NB-3^{-/-} mice. **(B–I)** Representative images of sagittal sections showing the sRST axons in NB-3^{+/+} **(B–E)** and NB-3^{-/-} **(F–I)** mice 84dpi. **(C–E and G–I)** High-magnification images of boxed areas in **(B and F)**, respectively. The arrows indicate the spinal lesion sites; the white dashed line indicates the regenerative sRST axons extending into the distal spinal cord; the asterisks indicate the lesion epicenters. **(J)** Quantification of an intensity index for sRST axons at certain distances from the lesion borders as in **(B and F)**. Data are presented as the mean \pm SEM. * $p < 0.01$; two-way ANOVA followed by Fisher's LSD. Scale bars, 200 μ m **(B and F)** and 50 μ m **(C–E, G–I)**.

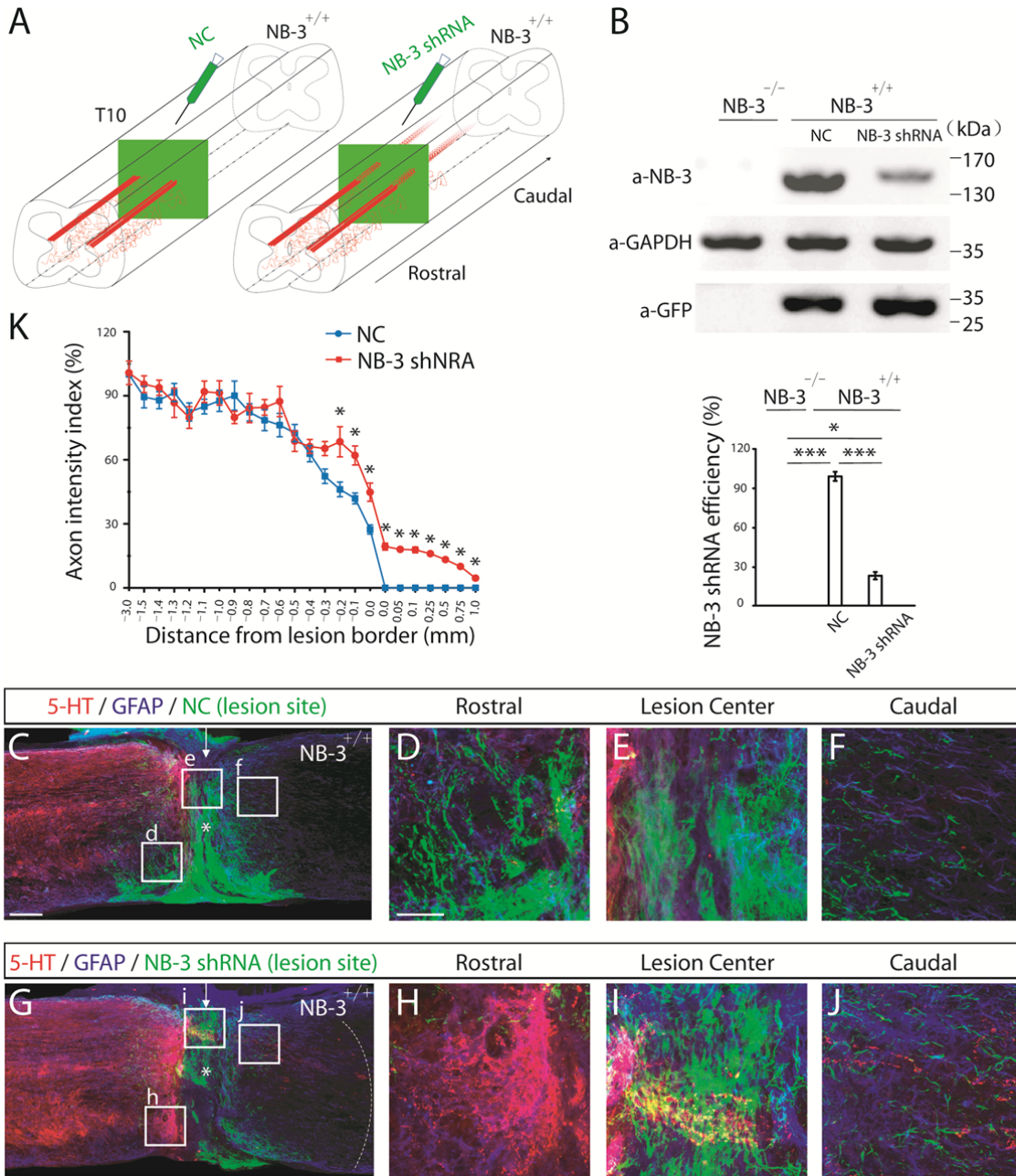


Fig. 3. Knockdown of NB-3 expression at the spinal lesion site leads to enhanced regrowth of post-traumatic sRST axons. **(A)** Diagram of sRST axons at the spinal lesion sites of NB-3^{+/+} mice infected with LV-NC-GFP or LV-NB-3 shRNA-GFP. **(B)** To validate the constructs LV-NC-EGFP and LV-NB-3 shRNA-EGFP, spinal tissues from appropriately infected mice were dissociated and analyzed for expression of NB-3, GAPDH, and GFP by western blotting. Data are presented as the mean ± SEM. * $p < 0.01$, and *** $p < 0.0001$; one-sample t-test. **(C–J)** Sagittal sections showing the sRST axons in injured spinal cords following spinal injection of

LV-NC-GFP (**C–F**) and LV-NB-3 shRNA-GFP (**G–J**) in NB-3^{+/+} mice 84dpi. **D–F** and **H–J**: High-magnification images of boxed areas in (**C** and **G**), respectively. The arrows indicate the spinal lesion sites; the white dashed line indicates the regenerative sRST axons extending into the distal spinal cord; the asterisks indicate the lesion epicenters. (**K**) Quantification of the intensity index of sRST axons at certain distances from the lesion borders as in (**C** and **G**). Data are presented as the mean \pm SEM. * $p < 0.01$; multiple t tests and two-way ANOVA followed by Fisher's LSD. Scale bars, 200 μm (**C** and **G**) and 50 μm (**D–F**, **H–J**).

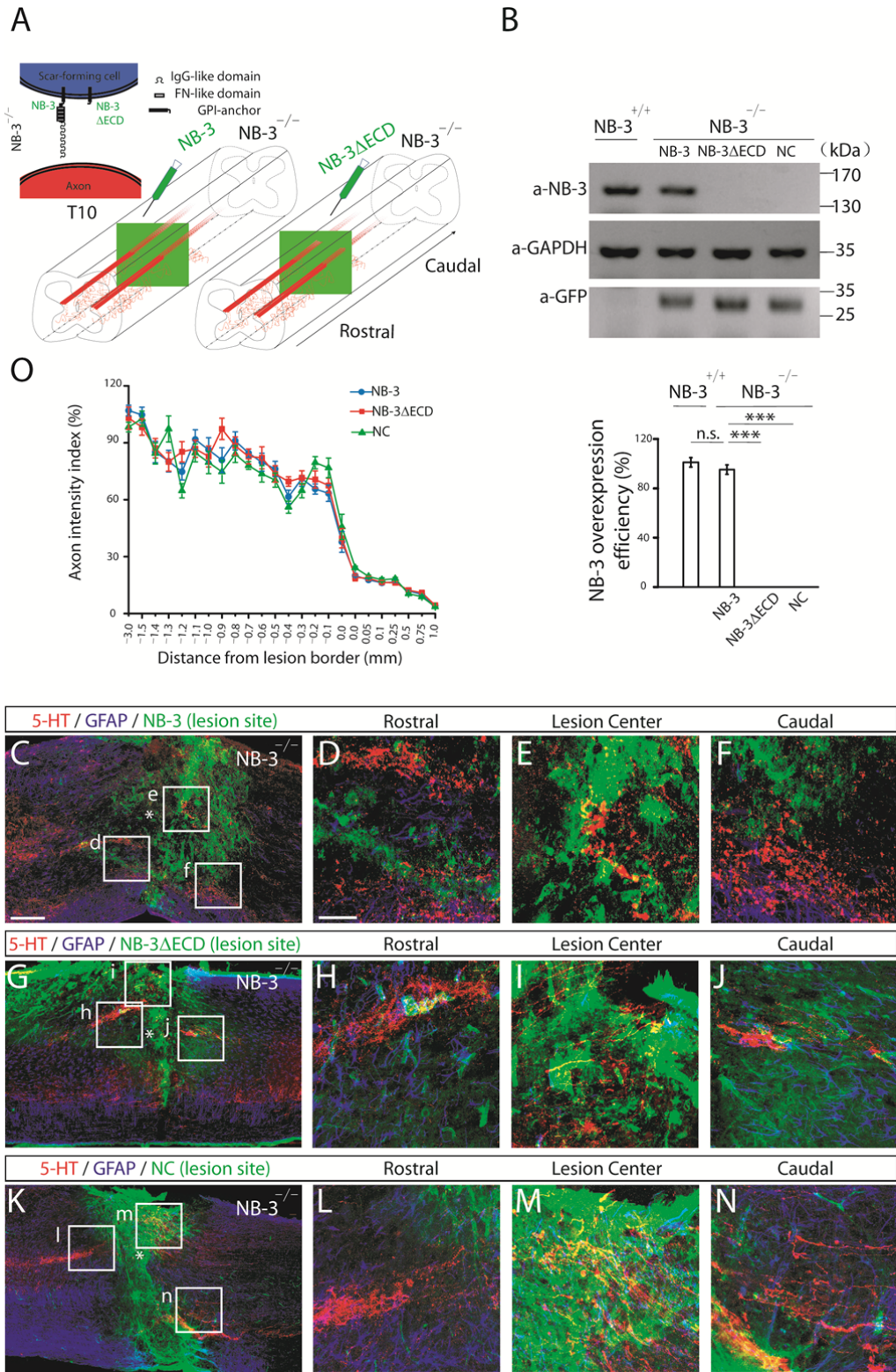


Fig. 4. Regrowth of post-traumatic sRST axons was not interrupted by overexpression of NB-3 only at the spinal lesion site in NB-3-deficient mice. **(A)** Diagram of regrowing sRST

axons at the spinal lesion sites of NB-3^{-/-} mice infected with LV-NB-3-EGFP or LV-NB-3ΔECD-EGFP. **(B)** To validate the constructs LV-NB-3-EGFP, LV-NB-3ΔECD-EGFP, and LV-NC-EGFP, spinal tissues from appropriately infected mice were dissociated and analyzed for expression of NB-3, GAPDH, and GFP by western blotting. Data are presented as the mean ± SEM, *n.s.*, not significant; *** $p < 0.0001$; one-sample t-test. **(C–N)** Sagittal sections showing the sRST axons in injured spinal cords following injection of LV-NB-3-EGFP **(C–F)** or LV-NB-3ΔECD-EGFP **(G–J)** or LV-NC-EGFP **(K–N)** into the lesion epicenter in NB-3^{-/-} mice 84dpi. **(D–F, H–J, L–N)** High-magnification images of boxed areas in **(C, G, K)**, respectively. The asterisks indicate the lesion epicenters. **(O)** Quantification of the intensity index of sRST axons at certain distances from the lesion borders as in **(C, G, K)**. Data are presented as the mean ± SEM; multiple t tests and two-way ANOVA followed by Fisher's LSD. Scale bars, 200 μm **(C, G, K)** and 50 μm **(D–F, H–J, L–N)**.

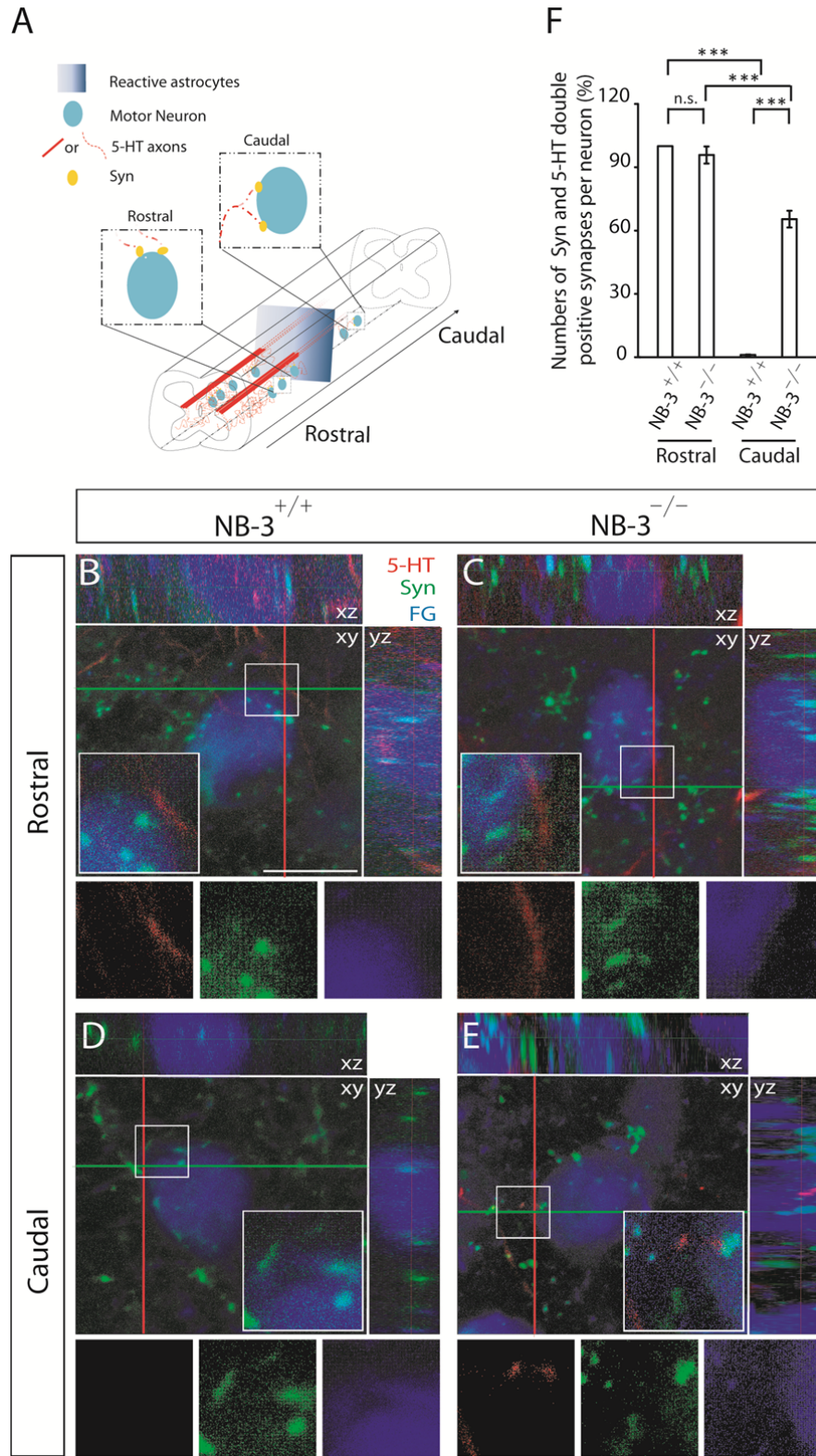


Fig. 5. Synapse reformation in NB-3-deficient mice after SCI. (A) Detection of synapse reformation between regenerative serotonergic axons and motor neurons in the injured

spinal cord 0.5 mm rostral to the lesion site and 0.5 mm caudal to the lesion site. **(B–E)** sRST axons, MNs, and the synapses that reformed between them were detected by co-immunostaining for 5-HT (red) and syn (green), along with FG (blue) labeling. Representative images of coronal sections showing synapse formation between the sRST axonal terminals and MNs at 0.5 mm rostral (**B** and **C**) and 0.5 mm caudal (**D** and **E**) to the spinal lesion site of NB-3^{+/+} (**B** and **D**) and NB-3^{-/-} (**C** and **E**) mice. Cross-lines indicate the position of xz (green) and yz (red) planes of interest. **(F)** Quantification of the number of synapses between sRST axonal terminals and MNs per neuron in each group as in **(B–E)**. Data are presented as the mean \pm SEM. *n.s.*, not significant; *** $p < 0.0001$; one-sample t-test. Scale bar, 30 μ m (**B–E**).

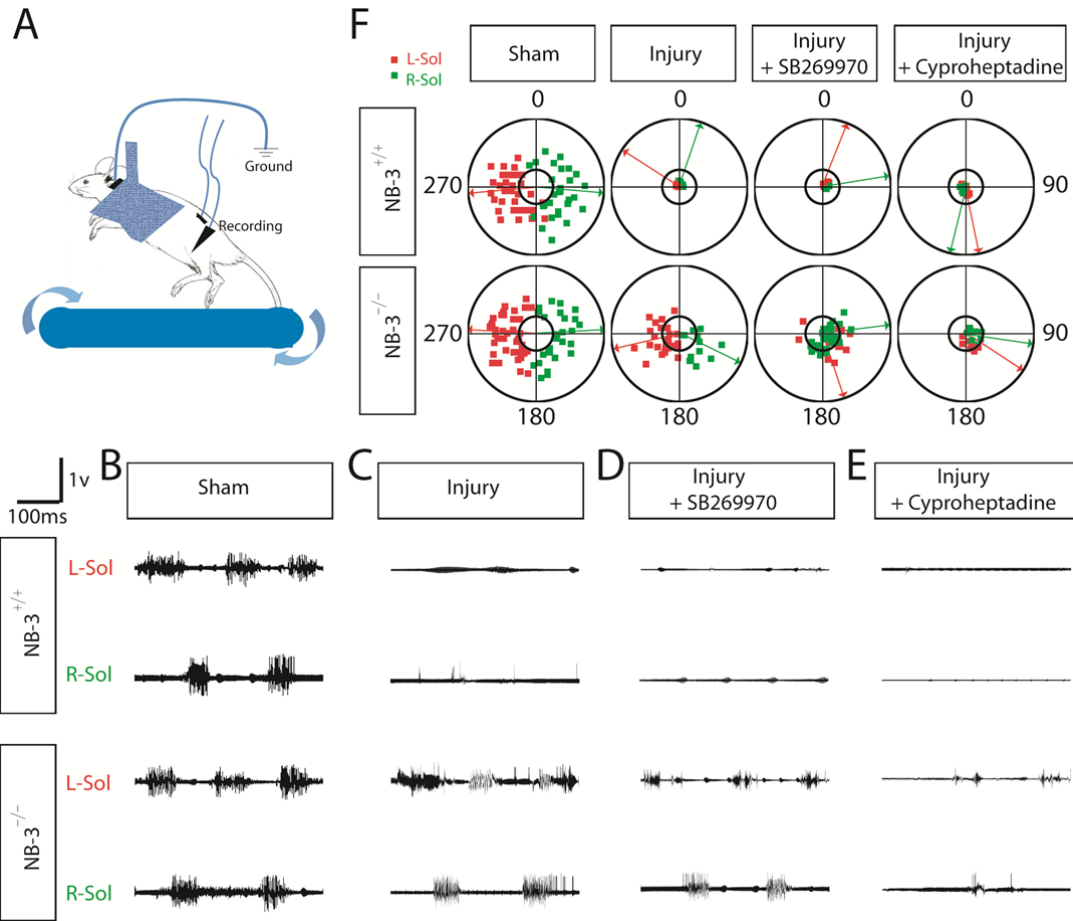
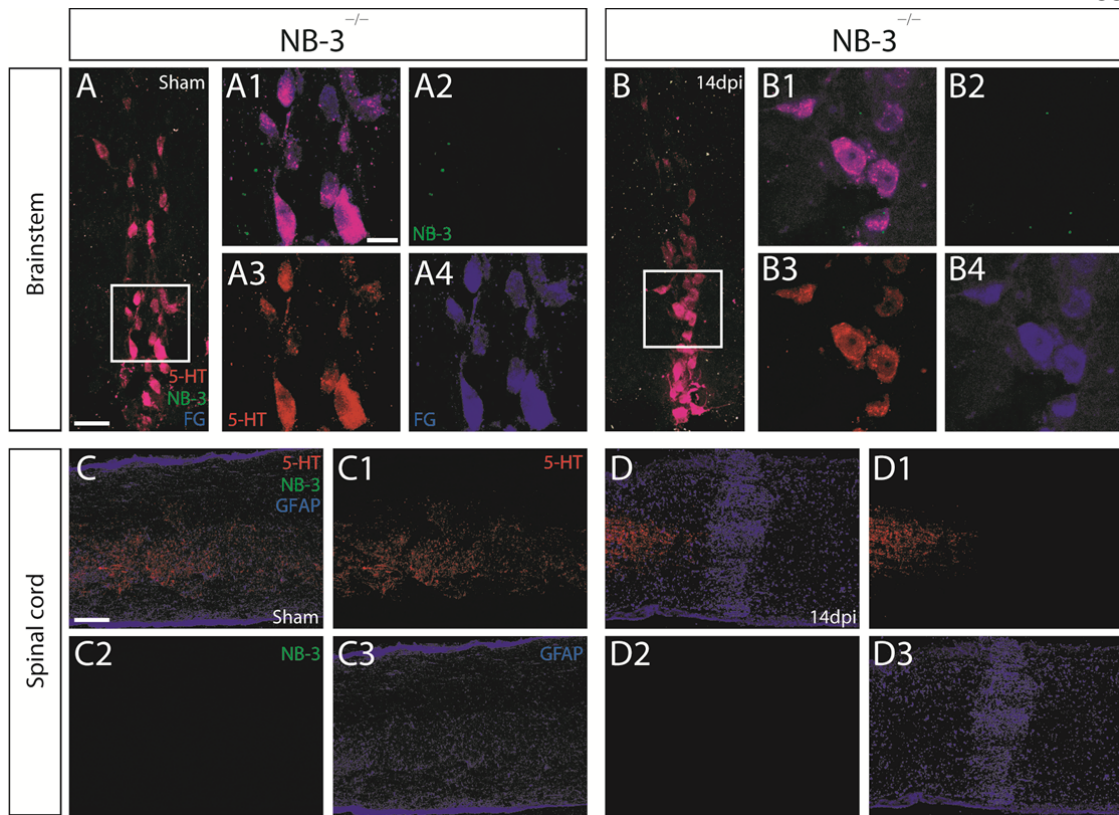
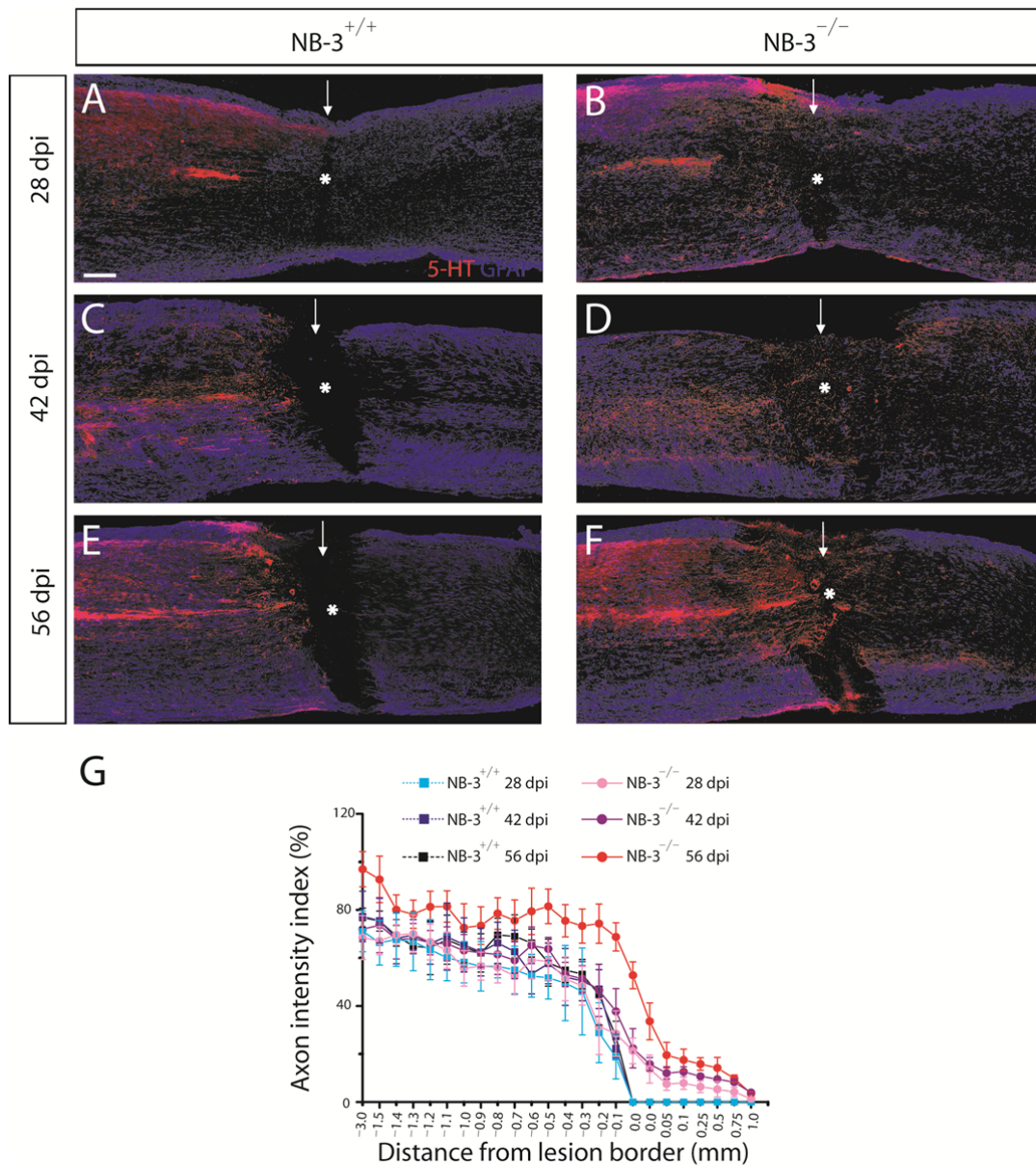


Fig. 6. Restoring muscle contraction and motor coordination in NB-3-deficient mice after SCI. **(A)** The test of locomotion recovery was performed with a rehabilitation facility as shown. **(B–E)** In each group of NB-3^{+/+} and NB-3^{-/-} mice, the muscle contraction and left-right coordination of both soleus muscles (L, left; R, right) were recorded in sham-operated **(B)** and injured mice **(C, D, and E)** 84dpi. Recording was performed immediately after SB269970 **(D)** and cyproheptadine **(E)** were intrathecally applied. **(F)** Quantification of EMG data to analyze the phasing of EMG firing during locomotion, which are represented by circular polar plots. The red and green dots indicate the mean onset phases of consecutive EMG bursts in the left and right soleus, respectively, in a single test. The length of the r (ranging from the origin point to each dot) indicates the clustering of the peak preferred phase around the mean phase. A smaller p -value (< 0.05) indicates more uniformity of data samples (the Rayleigh circular test is applied to test the uniformity of data samples). Dots outside the inner circle indicate $p < 0.05$ and are indicative of rhythmic movements in

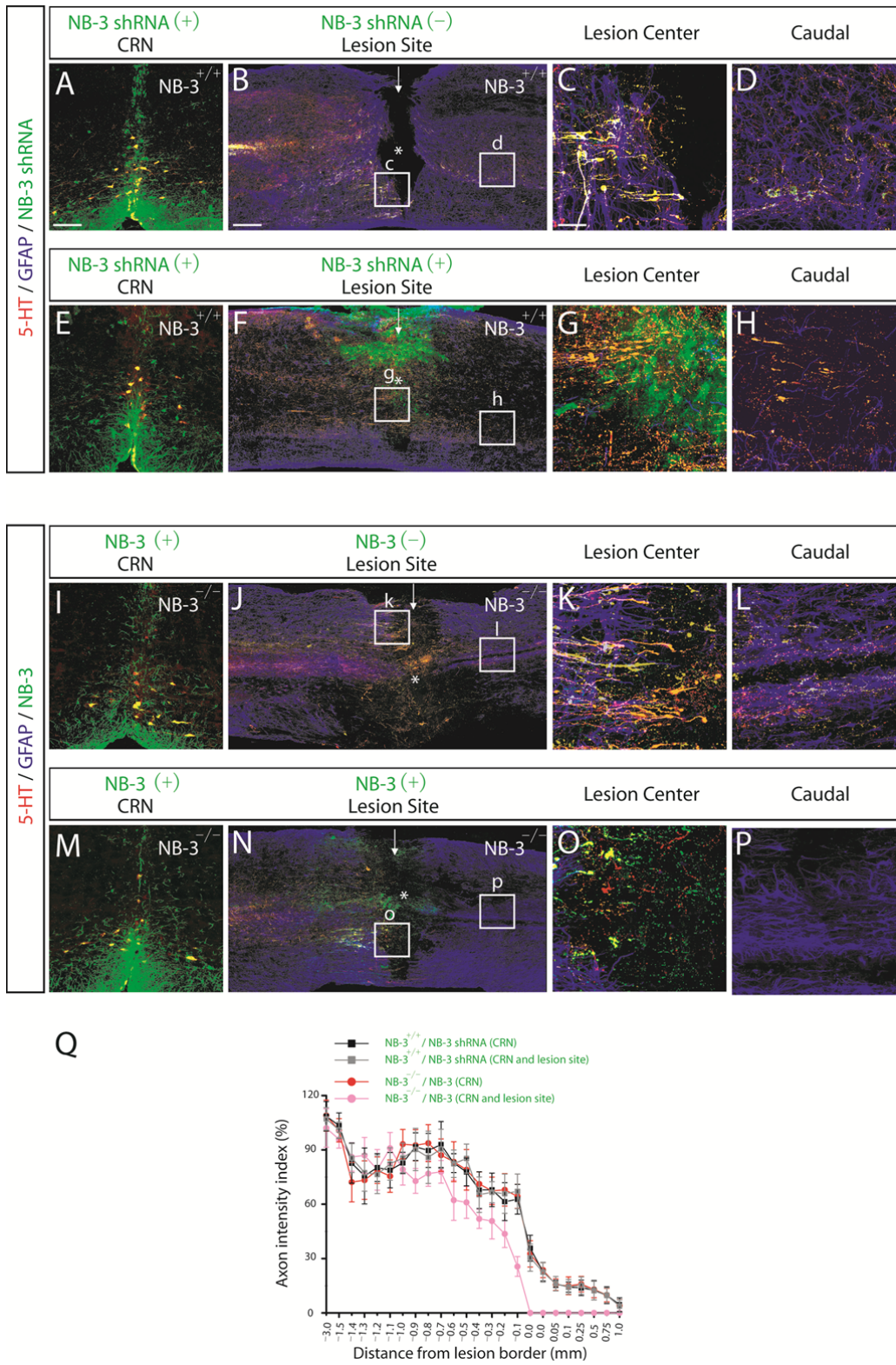
each hindlimb. The closer a dot is to the outer circle, the smaller its corresponding p -value is. The red and green arrow phases indicate the mean onset phases of all the left and right EMG bursts, respectively, in all tests. Synchrony of EMG burst onsets is reflected by a 0° difference in arrow phases in the polar plots, and alternation is reflected by a 180° difference in arrow phases; other angle differences in arrow phases are indicative of intermediate phases of synchrony and alternation.



Supplementary Fig. 1. Specificity of NB-3 antibody testing in somas of the sRST in NB-3^{-/-} mice after SCI. (A and B) Co-immunostaining for 5-HT (red) and NB-3 (green) in FG-labeled sRST somas (blue) in sham-operated (A) and injured (B) NB-3^{-/-} mice 14 dpi. (A1 and B1): High-magnification images of boxed areas in (A and B), respectively, that were split into individual channels (A2–A4 and B2–B4). (C and D) Co-immunostaining for GFAP (blue), NB-3 (green), and 5-HT (red) in spinal cords from sham-operated (C) and injured (D) NB-3^{-/-} mice 14 dpi. (C1–C3 and D1–D3): images that were split into individual channels in (C and D), respectively. Scale bars, 80 μm (A and B), 40 μm (A1–A4 and B1–B4), and 200 μm (C–D, C1–C4, D1–D4).



Supplementary Fig. 2. Analysis of time course of axonal extension in NB-3^{+/+} and NB-3^{-/-} mice after SCI. (A–F) Representative images of sagittal sections showing the sRST axons in NB-3^{+/+} (A, C, and E) and NB-3^{-/-} (B, D, and F) mice at 28 dpi (A and B), 42 dpi (C and D), and 56 dpi (E and F). The arrows indicate the spinal lesion sites; the asterisks indicate the lesion epicenters. (G) Quantification of an intensity index for sRST axons at certain distances from the lesion borders as in (A–F). Data are presented as the mean ± SEM; two-way ANOVA followed by Fisher’s LSD. Scale bars, 200 μm (A–F).



Supplementary Fig. 3. Blocking NB-3 expression in the CRN and/or spinal lesion site leads to enhanced regrowth of post-traumatic sRST axons. (A–H) Sections showing the sRST

axons in injured spinal cords following injection of LV-NB-3 shRNA-GFP into the CRN alone (**A** and **B**) or into both the raphe nucleus and spinal lesion site (**E** and **F**) of NB-3^{+/+} mice 84 dpi. (**C** and **D**) and (**G** and **H**) High-magnification images of boxed areas in (**B**) and (**F**), respectively. (**I–P**) Sections showing the sRST axons in injured spinal cords following injection of LV-NB-3-EGFP into the raphe nucleus alone (**I** and **J**) or into both the CRN and spinal lesion site (**M** and **N**) in NB-3^{-/-} mice 84 dpi. (**K** and **L**) and (**O** and **P**) High-magnification images of boxed areas in (**J**) and (**N**), respectively. The arrows indicate the spinal lesion sites; the asterisks indicate the lesion epicenters. (**Q**) Quantification of the intensity index of sRST axons at certain distances from the lesion borders as in (**B**, **F**, **J**, and **N**). Data are presented as the mean \pm SEM; multiple t tests and two-way ANOVA followed by Fisher's LSD. Scale bars, 100 μ m (**A**, **E**, **I**, and **M**), 200 μ m (**B**, **F**, **J**, and **N**), and 50 μ m (**C**, **D**, **G**, **H**, **K**, **L**, **O**, and **P**).